# Pump induced birefringence in dual-polarization fiber grating lasers

**Linghao Cheng (程凌浩)*, Yunbo Li (李云波), Yizhi Liang (梁贻智), Hao Liang (梁 浩), and Bai-Ou Guan (关柏鸥)**

*Institute of Photonics Technology, Jinan University, Guangzhou 510632, China*
**Corresponding author: chenglh@ieee.org*

Received January 14, 2017; accepted March 3, 2017; posted online March 29, 2017

Birefringence is critical in dual-polarization fiber-laser-based fiber-optic sensing systems, as it directly determines the beat frequency between the two polarizations. A study of pump induced birefringence in dual-polarization fiber lasers is presented here, which shows that the pump induced birefringence is a result of the interplay among pump induced refractive index change, laser dynamics, and anisotropy inside fiber lasers. For erbium-doped fiber lasers, pumping at 1480 nm is better than pumping at 980 nm in lower pump induced birefringence. Moreover, injection at 532 nm for an adequately long enough time can permanently reduce anisotropy and, hence, reduce pump induced birefringence.

*OCIS codes: 060.2370, 280.3420.*
*doi: 10.3788/COL201715.060602.*

Dual-polarization fiber lasers are very popular in fiber-optic sensing because they convert optical frequency changes to frequency variations in the radio frequency (RF) band and permit interrogations in the electronic domain, which can be faster and more cost effective than their counterparts in the optical domain[1–4]. For such fiber-optic sensing schemes based on dual-polarization fiber lasers, birefringence is critical, as the RF frequency variation is directly determined by the birefringence, which should reflect the quantity of the expected measurands. Therefore, intrinsic birefringence of fiber lasers should be as stable as possible. Otherwise, intrinsic birefringence will interfere with measurements, resulting in inaccurate measurements.

Birefringence is a spatial anisotropy of the refractive index. Therefore, if the refractive index is changed for some reason, potentially, birefringence can also be altered for the same reason. For erbium-doped fiber (EDF) lasers, the absorption and emission spectra of EDF is changed under pumping. Consequently, the refractive index is also changed due to the well-known Kramers–Kronig relation, which is known as the pump induced refractive index change[5–8]. Due to anisotropy inside EDFs, such pump induced refractive index changes can also be anisotropic, resulting in pump induced birefringence as well. However, for fiber lasers, laser dynamics are also involved in the refractive index and birefringence change, since population distribution among various energy levels should follow the laser dynamics. Therefore, for dual-polarization fiber lasers, a pump induced birefringence change can be very different for different pumping schemes because different energy levels are involved in laser dynamics.

Although pump induced refractive index change has been studied extensively for EDFs, pump induced birefringence and its interaction with fiber lasers still need further investigation, especially for a dual-polarization fiber-laser-based fiber-optic sensing system, because high measurement accuracy is highly desired. In this Letter, we present a study of pump induced birefringence for dual-polarization fiber lasers. It shows that pump induced birefringence is pumping scheme dependent. For EDF lasers, a pumping scheme at 1480 nm is better than one at 980 nm in lower pump induced birefringence. Moreover, injection at 532 nm for an adequately long enough time is also effective in reducing pump induced birefringence through permanently lowering anisotropy.

Some other effects can result in a birefringence change, such as the thermal effect and the Kerr electro-optic effect[9–11]. We have discussed and compared all of these sources and found that pump induced birefringence is the dominant one[12]. Therefore, we only focus on this effect.

For an EDF, two pumping wavelengths, 1480 and 980 nm, are commonly used to generate the emission at the band around 1530 nm. For the pumping scheme at 1480 nm, the optical transitions responsible for the absorption and the emission are between the $^4I_{15/2}$ ground states (level 1) and the $^4I_{13/2}$ metastable states (level 2). The complex susceptibility associated with these transitions results in additional refractive index $n_{12}$ and linear absorption coefficient $\alpha_{12}$ through the real and imaginary parts of the complex susceptibility, respectively. Because the real and the imaginary parts of the complex susceptibility are related by the Kramers–Kronig transform, $n_{12}$ can then be obtained through the corresponding absorption coefficient $\alpha_{12}$ according to[13]

$$n_{12}(\omega) = \frac{c}{\pi}\mathrm{P.V.}\int_0^{+\infty} \frac{\alpha_{12}(\omega')}{\omega'^2 - \omega^2}\,\mathrm{d}\omega', \tag{1}$$

where $c$ is the speed of light in the vacuum, and P.V. stands for the Cauchy principle value. Because $\alpha_{12}$ is proportional

 

to $N_{12}$ where $N_{12}$ is the population difference between level 1 and 2, $n_{12}$ is then also proportional to $N_{12}$. For a fiber laser, $N_{12}$ has to follow laser dynamics as well, which is then determined by the intrinsic loss inside the laser cavity. If a Lorentzian lineshape is assumed, $N_{12}$ can be expressed as[14]

$$N_{12} = \frac{2\pi\alpha_r}{\lambda^2}, \tag{2}$$

where $\lambda$ is the emission wavelength, and $\alpha_r$ is the distributed loss coefficient inside the laser cavity. Therefore, $n_{12}$ is also determined by $\alpha_r$. Since the anisotropy of $\alpha_r$ is basically not pump dependent, pump induced birefringence should not be observed for dual-polarization fiber lasers operating on the transitions just between levels 1 and 2, such as those with a pumping scheme at 1480 nm.

For pumping schemes at 980 nm, the scenario is much different because more energy levels are involved in laser dynamics. The population is pumped from the $^4I_{15/2}$ ground states to the short-lived $^4I_{11/2}$ states (level 3) from which the population relaxes to the metastable states to generate the emission at the band around 1530 nm. When the pump is sufficiently intense, excited-state absorption (ESA) becomes prominent, which arises from a sequential two-photon absorption at 980 nm to pump the population from the $^4I_{15/2}$ ground states to the $^4F_{7/2}$ states through the intermediate $^4I_{11/2}$ states[15,16]. From the $^4F_{7/2}$ states, the population experiences a fast decay to the $^4F_{9/2}$, the $^4S_{3/2}$, and the $^4H_{11/2}$ states (level 4) and produces emissions at around 690, 550, and 525 nm, respectively. Therefore, with pumping schemes at 980 nm, the population is redistributed among four energy levels and produces more emissions besides the one at around 1530 nm. Because of the ESA, the strength of the absorption at 980 nm is also changed. All of these population changes in the energy levels and their corresponding absorptions and emissions contribute to the refractive index change. Moreover, because the laser cavity is transparent to these new absorptions and emissions, their corresponding population distribution on the energy levels is not determined by the intrinsic loss inside the laser cavity. For example, by solving rate equations, the population difference between levels 4 and 3 can be approximated as[12]

$$N_{34} = -\frac{\tau_{32}}{2\tau_{21}}(N_a + N_{12}) - N_{12}W_{21}\tau_{32} - \tau_{43}(R_{13} - R_{34}), \tag{3}$$

where $N_{ij}$ stands for the population difference between levels $j$ and $i$, $N_a$ is the sum of the population on all levels, $\tau_{ij}$ stands for the decay time from levels $i$ and $j$, $R_{ij}$ is the pumping rate from levels $i$ to $j$, and $W_{ij}$ is the probability density of the stimulated emission from levels $i$ to $j$. It then shows that the population difference between energy levels is dependent on the dopant concentration and the pumping rate except the one between level 2 and level 1.

However, the pump induced refractive index change does not necessarily result in a birefringence change. Anisotropy has to be involved in the process so that the population differences, as shown by Eq. (3) and, hence, their corresponding contributions to the refractive index change, can be polarization dependent. For EDFs, such polarization dependent anisotropy manifests as polarization dependent gain (PDG)[17,18], which, together with the polarization of the pump, makes the dopant concentration and the pumping rate, as shown in Eq. (3), pump polarization dependent. For example, the population difference between two orthogonal polarization states for the population difference between levels 4 and 3 can be obtained as

$$\Delta N_{34} = -\frac{\tau_{32}}{2\tau_{21}}\Delta N_a - \tau_{43}(\Delta R_{13} - \Delta R_{34}), \tag{4}$$

where $\Delta$ denotes the difference between the two orthogonal polarization states. Therefore, with anisotropy present, the corresponding contribution to the birefringence change is also pump polarization dependent, resulting in pump induced birefringence. Because the pump induced birefringence is polarization dependent, a sinusoid dependence on the pump polarization state is then expected.

An experiment setup to study pump induced birefringence in dual-polarization fiber lasers is shown in Fig. 1. The dual-polarization fiber laser under investigation is a short-cavity distributed Bragg reflector (DBR) fiber laser fabricated on an EDF (FiberCore-M12-980-125) with two fiber Bragg gratings (FBGs) spaced by 5 mm. The FBGs are 5 mm long and are inscribed on the EDF by a 193 nm excimer. The pump laser of the fiber laser is linearly polarized. A manual polarization controller composed of rotatable waveplates is used to convert the linear polarization of the pump laser output to the desired polarization states. Provided that the input polarization is a linear polarization, and the two circular polarizations are the two poles of Ponicaré sphere, a half-waveplate can rotate it along the equator, and a quarter-waveplate can rotate it along longitude lines, and, hence, all of the polarizations can be reached[19,20]. The beat note at about 400 MHz is generated by photodetecting the fiber laser output and monitored by an RF spectrum analyzer. Because the beat note frequency is

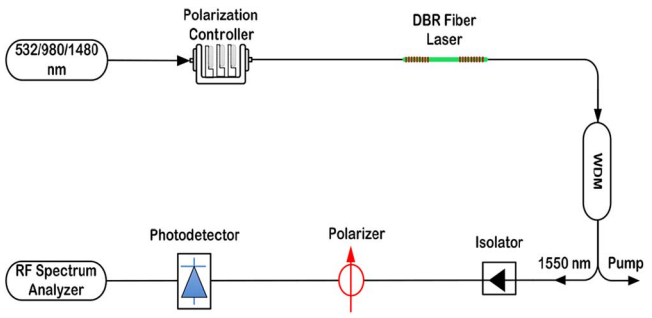


Fig. 1. Experiment setup. WDM, wavelength division multiplexer.

proportional to the birefringence inside the laser cavity, its variation reflects the birefringence change.

Pump induced birefringence for a linearly polarized pump is first studied. The beat note frequencies at different pump polarization orientations are shown in Fig. 2 for two cases of pumping at 980 and 1480 nm. The plane of pump polarization is rotated by a half-waveplate, and, hence, the polarization rotation angle shown in Fig. 2 is referred to as the half-waveplate rotation. Along with the polarization plane rotation angle, the beat note frequency varies according to the sinusoidal curves. When the orientation of the pump polarization aligns with one axis of the fiber, one peak or one valley of the frequency variation appears. The two axes of the fiber can then be determined. Note that the peaks and the valleys for 1480 nm pumping do not coincide with those for 980 nm pumping because the polarization rotation angle is referred to as the half-waveplate rotation instead of the two axes of the fiber. As the theoretical analysis expects, the beat note frequency variation for 1480 nm pumping is much smaller than that of 980 nm pumping because, for the 980 nm pumping, higher energy levels other than the $^4I_{15/2}$ ground states and the $^4I_{13/2}$ metastable states involved in the laser dynamics and the anisotropy resulted from the pump induced refractive index change, which manifests itself as a frequency variation. For 1480 nm pumping, only the $^4I_{15/2}$ ground states and the $^4I_{13/2}$ metastable states involved in the laser dynamics and the population distribution among energy levels is basically fully determined by the intrinsic laser cavity loss, which is quite stable regardless of the pump polarization change.

Birefringence induced by pump polarization states other than linear polarizations is also examined. Figure 3 shows a scan of the beat note frequency versus pump polarization states for the 980 nm pumping, which is actually a map of the Poincaré sphere with linear polarization states at the equator and circular polarization states at the poles. In Fig. 3, the $x$ axis and the $y$ axis stand for the longitude and the latitude of the Poincaré sphere, respectively, with the equator at the bottom of the figure.

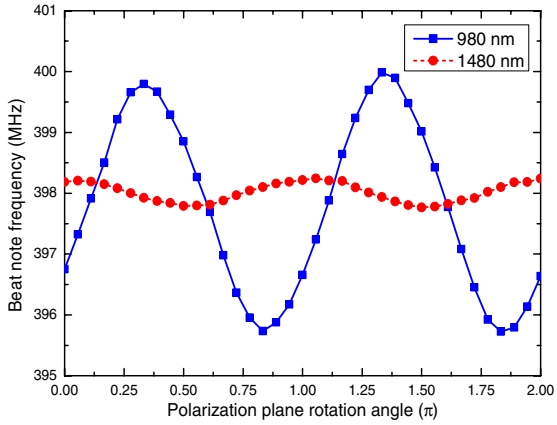


Fig. 2. Beat note frequencies versus linear polarization orientations of the pump.

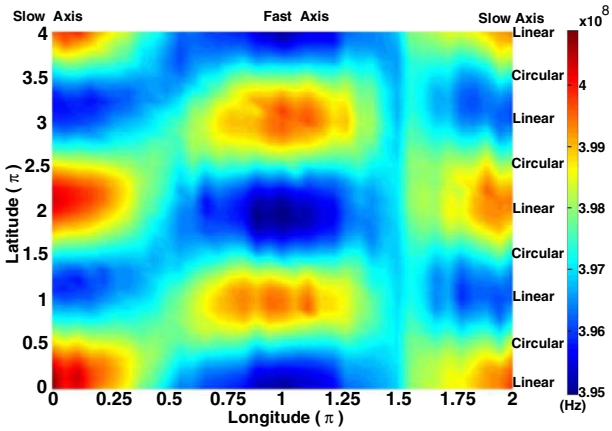


Fig. 3. Beat note frequency versus pump polarization states for pumping at 980 nm.

Because the two axes have been determined through the experiment shown in Fig. 2, the coordinates employed in Fig. 3 are referred to as the two axes of the fiber with the slow axis assumed to be at the origin point. Figure 3 shows that the peaks and valleys of the beat note frequency variation appear at linear polarization states launched along one of the two axes. For circular polarizations and linear polarizations with a $\pi/4$ orientation to the two axes, the beat frequency is at the medium of the two maxima.

The power of the beat note for various launched pump polarization states is also measured and shown in Fig. 4. Because the measurement takes a long time to complete, and the beat note power is easily disturbed by various environmental interferences, the results at each line of longitude are normalized according to the maximum of that line of longitude to remove disturbances. It shows that the maxima of the beat note power also appear at linear polarization states launched along one of the two axes. However, compared to the maxima of beat note frequency, the peaks and valleys are reversed for beat note power. The variation of beat note frequency and power at

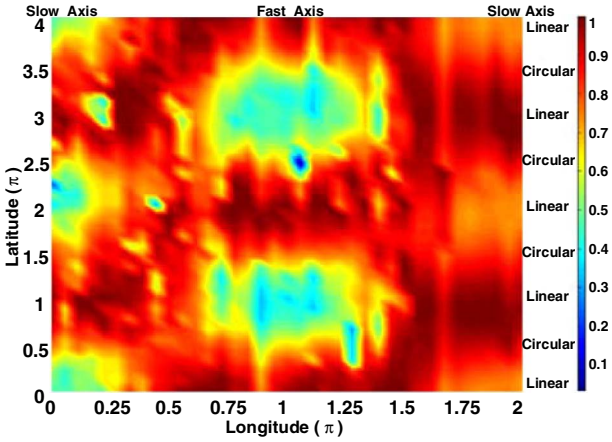


Fig. 4. Beat note power variation for different pump polarization states for pumping at 980 nm.

different pump polarization states is also measured for 1480 nm pumping, and results similar to Figs. 3 and 4 are obtained. The variation range of beat note power is roughly the same for both 980 and 1480 nm pumping. However, the variation range of beat note frequency is much smaller for 1480 nm pumping, which is about 1.13 MHz in contrast to 5.94 MHz for 980 nm pumping.

It has been shown that an injection of a green laser at 532 nm can reduce the pump induced birefringence for pumping at 980 nm[10]. Further investigation shows that such an injection has a profound effect on fiber anisotropy. An experiment is designed to demonstrate this, and the results are shown in Fig. 5. A new dual-polarization fiber grating laser is fabricated with a beat note frequency of about 440 MHz. Its pump induced birefringence is measured sequentially for different pumping schemes. 980 nm pumping is first employed, and the frequency variation range is about 4 MHz. Then, without surprise, 1480 pumping shows a much smaller frequency variation range of less than 1 MHz. 980 nm pumping is then employed again, and the range is as large as the first measurement. A green laser at 532 nm is then injected into the fiber laser together with a 980 nm pump laser, and the variation range becomes smaller, as expected. After injection at 532 nm for about 120 m without 980 nm pumping present, the fiber laser is then pumped again at 980 nm alone. The pump induced birefringence is much smaller now, resulting in a frequency variation range of about 1 MHz. The average beat note frequency is also significantly dropped to about 10 MHz. It then shows that the injection at 532 nm reduces the fiber anisotropy, which is similar to annealing by the heat treatment of fiber lasers.

It is then inferred from experimental results that the pump induced birefringence may stem from the inscription of FBGs by the excimer. The ultraviolet (UV) radiation of the excimer makes higher energy states partially populated. Because the UV radiation is polarized, additional anisotropy is then introduced[21,22]. Such anisotropy involved in laser dynamics is to be shown as pump induced birefringence. Provided the injection time is adequately long enough, the injection at 532 nm can make the population at higher energy states return to the ground states, resulting in reduced anisotropy and, hence, reduced pump induced birefringence.

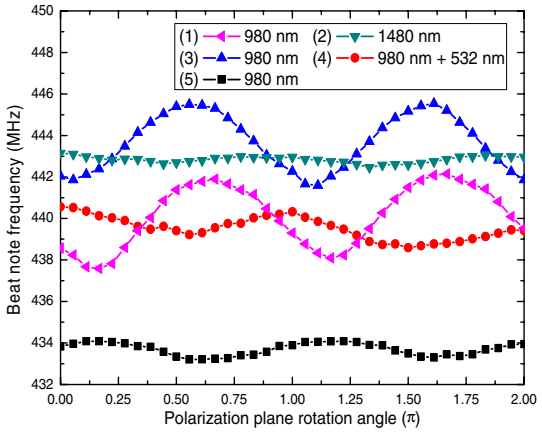


Fig. 5. Beat note frequency variation for sequential pumping at different wavelengths.

Therefore, to reduce pump induced birefringence, two methods can be employed. The first one is to reduce the anisotropy of fiber lasers by injection at 532 nm or annealing through heat treatment for an adequately long enough time. The second one is to pump at 1480 nm instead of 980 nm to prevent higher energy states from being involved in laser dynamics.

Pump induced birefringence in dual-polarization fiber grating lasers is studied through theoretical analysis and experiments, which is shown to be a result of the interplay among pump induced refractive index change, laser dynamics, and anisotropy inside fiber lasers. It has a maxima when the pump is linearly polarized along one of the two axes of fiber lasers. Pumping at 1480 nm produces much smaller birefringence than that of pumping at 980 nm, because higher energy states do not involve laser dynamics. Moreover, injection at 532 nm results in a similar effect as that of annealing through heat treatment to reduce anisotropy and, hence, reduce pump induced birefringence.

This work was supported by the National Natural Science Foundation of China (Nos. 11474133, 61235005, and 61675091) and the Natural Science Foundation of Guangdong Province of China (No. 2014A030310419).

## References

1. B.-O. Guan, L. Jin, Y. Zhang, and H.-Y. Tam, J. Lightwave Technol. **30**, 1097 (2012).
2. Y. Zhang, B.-O. Guan, and H.-Y. Tam, Opt. Express **17**, 10050 (2009).
3. Z. Liu and H.-Y. Tam, Chin. Opt. Lett. **14**, 120007 (2016).
4. Z. Kuang, L. Cheng, Y. Liang, H. Liang, and B.-O. Guan, Chin. Opt. Lett. **14**, 050602 (2016).
5. E. Desurvire, J. Lightwave Technol. **8**, 1517 (1990).
6. C. Thirstrup, Y. Shi, and B. Pálsdóttir, J. Lightwave Technol. **14**, 732 (1996).
7. S. C. Fleming and T. J. Whitley, IEEE J. Quantum Electron. **32**, 1113 (1996).
8. A. Quintela, M. A. Quintela, C. Jauregui, and J. M. Lopez-Higuera, IEEE Photon. Technol. Lett. **19**, 732 (2007).
9. L. Mousavi, M. Sabaeian, and H. Nadgaran, Opt. Commu. **300**, 69 (2013).
10. L. Mousavi and M. Sabaeian, Braz. J. Phys. **46**, 481 (2016).
11. A. Jahromi, M. Sabaeian, and H. Nadgaran, Opt. Commun. **311**, 134 (2013).
12. Y. Liang, Q. Yuan, L. Jin, L. Cheng, and B.-O. Guan, IEEE J. Sel. Top. Quantum Electron. **20**, 5600208 (2014).
13. M. J. F. Digonnet, R. W. Sadowski, H. J. Shaw, and R. H. Pantell, Opt. Fiber Technol. **3**, 44 (1997).
14. B. E. A. Saleh and M. C. Teich, *Fundamentals of Photonics* (Wiley-Interscience, 2007).
15. P. A. Krug, M. G. Sceats, G. R. Atkins, S. C. Guy, and S. B. Poole, Opt. Lett. **16**, 1976 (1991).

16. Y. Mita, T. Yoshida, T. Yagami, and S. Shionoya, J. Appl. Phys. **71**, 938 (1992).
17. P. Wysocki and V. Mazurczyk, J. Lightwave Technol. **14**, 572 (1996).
18. E. Ronnekleiv, M. N. Zervas, and J. T. Kringlebotn, IEEE J. Quantum Electron. **34**, 1559 (1998).
19. A. Hidayat, B. Koch, H. Zhang, V. Mirvoda, M. Lichtinger, D. Sandel, and R. Noé, Opt. Express **16**, 18984 (2008).
20. P. Cai, J. Wang, C. Wang, P. Zeng, and H. Li, Chin. Opt. Lett. **14**, 010009 (2016).
21. T. Erdogan and V. Mizrahi, J. Opt. Soc. Am. B **11**, 2100 (1994).
22. Y. Zhang, Y.-N. Tan, T. Guo, and B.-O. Guan, Opt. Express **19**, 218 (2010).